

Semiclassical description of electronically nonadiabatic dynamics via the initial value representation

Nandini Ananth, Charulatha Venkataraman, and William H. Miller

Department of Chemistry, University of California, Berkeley, California 94720-1460; Kenneth S. Pitzer Center for Theoretical Chemistry, University of California, Berkeley, California 94720-1460; and Chemical Sciences Division, Lawrence Berkeley National Laboratory, Berkeley, California 94720-1460

(Received 3 April 2007; accepted 25 June 2007; published online 30 August 2007)

The initial value representation (IVR) of semiclassical (SC) theory is used in conjunction with the Meyer-Miller/Stock-Thoss description of electronic degrees of freedom in order to treat electronically nonadiabatic processes. It is emphasized that the classical equations of motion for the nuclear and electronic degrees of freedom that emerge in this description are precisely the Ehrenfest equations of motion (the force on the nuclei is the force averaged over the electronic wave function) but that the trajectories given by these equations of motion do not have the usual shortcomings of the traditional Ehrenfest model when they are used within the SC-IVR framework. For example, in the traditional Ehrenfest model (a mixed quantum-classical approach) the nuclear motion emerges from a nonadiabatic encounter on an *average* potential energy surface (a weighted average according to the population in the various electronic states), while the SC-IVR describes the correct correlation between electronic and nuclear dynamics, i.e., the nuclear motion is on one potential energy surface or the other depending on the electronic state. Calculations using forward-backward versions of SC-IVR theory are presented to illustrate this behavior. An even more approximate version of the SC-IVR, the linearized approximation (LSC-IVR), is slightly better than the traditional Ehrenfest model, but since it cannot describe quantum coherence effects, the LSC-IVR is also not able to describe the correct correlation between nuclear and electronic dynamics. © 2007 American Institute of Physics. [DOI: 10.1063/1.2759932]

I. INTRODUCTION

Classical molecular dynamics (MD) simulations are the most common and generally applicable way to describe dynamical processes in large molecular systems. When electronically nonadiabatic processes are involved (those that involve transitions between different Born-Oppenheimer potential energy surfaces), it is natural to try to generalize MD simulations to deal with them. This has led to a variety of mixed quantum-classical (QC) models, where the electronic degrees of freedom are treated quantum mechanically via an electronic wave function determined by the time-dependent Schrödinger equation, and the nuclear degrees of freedom (dofs) classically as numerically computed classical trajectories. The time dependence for the electronic dofs comes from the dependence of the potential energy surfaces and their couplings on the nuclear coordinates, which vary with time along classical trajectories.

The various mixed QC models differ primarily in the forces or equivalently the effective potential surfaces that determine the classical motion of the nuclei. Most such approaches can be classified as either Ehrenfest (mean field) models or surface-hopping models. Tully¹ has given an excellent discussion of the differences of these two approaches as well as the strengths and weaknesses of each. Briefly, in Ehrenfest models one computes the force on the nuclei by averaging the electronic potential surface (matrix) using the instantaneous electronic wave function, while in surface-hopping approaches the force is determined from one (adia-

batic) potential surface or another, with instantaneous hops between different adiabatic surfaces permitted according to some hopping algorithm.

A positive feature of the Ehrenfest model is that it is a well-defined approximation, while surface-hopping models have a number of *ad hoc* features which, though physically reasonable, may be difficult to justify. A significant shortcoming of the Ehrenfest model is that the nuclear trajectories are determined by the average potential energy surface (PES) even in the asymptotic region of a scattering problem, where the nuclear trajectories should, of course, be determined by one PES or another depending on the electronic state. The mean field aspect of the Ehrenfest model is not able to describe this correlation.

A significant contribution to the theory was made by Neria and Nitzan² in pointing out that the failure of these mixed QC models results from the fact that the nuclear dofs are not described by a *wave function* but only as classical trajectories. Though their analysis was based only on the golden rule (lowest order perturbation theory), it correctly identified the problem and suggested some ways to try to overcome it, for instance, by assigning a Gaussian wave packet (nuclear wave function) to the classical trajectories of the nuclei. Prezhdo and Rossky³ picked up on this idea and made good use of it, and more recently Hack and Truhlar⁴ have also used it to construct more refined surface-hopping models. (Both of these groups have focused on determining a

decoherence time for the nuclear wave function to collapse to one electronic PES or another.)

The initial value representation (IVR) of semiclassical (SC) theory⁵ provides a natural and correct description of electronically nonadiabatic processes. This is perhaps not surprising since the nuclear (and electronic) dofs do have a wave function in the SC description. It is interesting, though, that *the equations of motion that determine the nuclear trajectories are precisely the Ehrenfest equations*, but by processing the trajectories through the SC theory, the nuclear motion emerges (in a scattering problem, as the present examples are) on one PES or another, not on the average PES.

To apply the SC theory to a vibronic system (one with electronic and nuclear dofs), we use the Meyer-Miller-Stock-Thoss (MM-ST) classical analog model for the electronic degrees of freedom. This replaces the N electronic states involved in the process by N classical degrees of freedom, specifically a harmonic oscillator for each electronic state. All dofs—those of the nuclei and those of the N “electronic” oscillators—are then treated semiclassically via the IVR methodology (involving trajectories computed in the full coordinate and momentum spaces of nuclear and electronic dofs). Though Meyer and Miller⁶ (MM) developed this classical model for the electronic degrees of freedom as an approximate way to be able to treat electronic and nuclear dynamics on an equal footing, the more recent derivation of the model by Stock and Thoss⁷ (ST) shows that it is actually not a *model* (i.e., approximation) but rather an exact *representation* of the full vibronic system. In other words, if one were to take the MM-ST vibronic Hamiltonian and implement it quantum mechanically, the exact vibronic dynamics would be obtained. The only approximation here is that it is implemented semiclassically via the IVR.

In a previous paper,⁸ we demonstrated that the approach described above captured transmission probabilities accurately for Tully’s¹ three model systems. In this paper, we further show that the IVR and some of its variations can indeed provide a complete dynamical picture of nonadiabatic systems both in terms of instantaneous populations of states as well as the quantum coherences between them. Section II first gives a brief summary of the MM-ST description of the electronic-nuclear system, and Sec. III does the same for the SC-IVR methodology. We utilize the forward-backward (FB) version of the IVR approach, which makes the calculations efficient and yet retains the ability to describe quantum coherence effects correctly. As seen in the examples treated in Sec. IV, if one makes the cruder linearized approximation to the SC-IVR (which reduces to the classical Wigner model), one loses the ability to describe coherence; the results of this linearized or LSC-IVR approximation become essentially those of the traditional Ehrenfest model, with the nuclear trajectory emerging (incorrectly) on the average of the electronic PESs. With the more rigorous FB-IVR, however, the nuclear trajectory emerges on one potential energy surface or the other.

II. THE MM-ST VIBRONIC HAMILTONIAN

MM (Ref. 6) arrived at their classical model for electronic degrees of freedom in the following way. If

$V_{kk'}(\mathbf{R}(t)), k, k' = 1, \dots, N$, is the $N \times N$ diabatic electronic potential matrix for N electronic states, where the nuclear coordinates follow some given trajectory $\mathbf{R}(t)$, and the electronic wave function is given by an expansion in terms of the N diabatic electronic states,

$$|\Psi_{\text{el}}(t)\rangle = \sum_{k=1}^N |\phi_k\rangle c_k(t), \quad (2.1)$$

then the time-dependent Schrödinger equation for the electronic amplitudes reads (with $\hbar = 1$)

$$i\dot{c}_k(t) = \sum_{k'=1}^N V_{kk'}(\mathbf{R}(t))c_{k'}(t). \quad (2.2)$$

MM noted that if the complex-valued electronic amplitudes $c_k(t)$ were written in terms of a magnitude and phase,

$$c_k = \sqrt{n_k + \frac{1}{2}} e^{-iq_k}, \quad (2.3)$$

and (n_k, q_k) considered to be canonically conjugate action-angle variables (generalized coordinates and momenta), then Hamilton’s equations of motion for the electronic action-angle variables,

$$\begin{aligned} \dot{q}_k &= \frac{\partial H_{\text{el}}(\mathbf{n}, \mathbf{q}; t)}{\partial n_k}, \\ \dot{n}_k &= -\frac{\partial H_{\text{el}}(\mathbf{n}, \mathbf{q}; t)}{\partial q_k}, \end{aligned} \quad (2.4)$$

are identical to the time-dependent Schrödinger equation of Eq. (2.2) if one defines the classical electronic Hamiltonian as

$$\begin{aligned} H_{\text{el}}(\mathbf{n}, \mathbf{q}; t) &= \sum_{k, k'=1}^N c_k^*(t) V_{kk'}(\mathbf{R}(t)) c_{k'}(t) \\ &= \sum_{k=1}^N n_k V_{kk}(\mathbf{R}(t)) + 2 \sum_{k < k'=1}^N V_{kk'}(\mathbf{R}(t)) \\ &\quad \times \sqrt{n_k + \frac{1}{2}} \sqrt{n_{k'} + \frac{1}{2}} \cos(q_k - q_{k'}), \end{aligned} \quad (2.5)$$

where the constant term (independent of n_k, q_k) $\frac{1}{2} \sum_{k=1}^N V_{kk}$ has been subtracted in obtaining Eq. (2.5). When the nuclear kinetic energy, $\mathbf{P}^2/2\mu$, is now added to the electronic Hamiltonian of Eq. (2.5), the full classical vibronic Hamiltonian is then given in terms of the nuclear (\mathbf{R}, \mathbf{P}) and electronic (\mathbf{n}, \mathbf{q}) coordinates and momenta as

$$\begin{aligned} H(\mathbf{P}, \mathbf{R}, \mathbf{n}, \mathbf{q}) &= \frac{\mathbf{P}^2}{2\mu} + \sum_{k=1}^N n_k V_{kk}(\mathbf{R}) + 2 \sum_{k < k'=1}^N V_{kk'}(\mathbf{R}) \\ &\quad \times \sqrt{n_k + \frac{1}{2}} \sqrt{n_{k'} + \frac{1}{2}} \cos(q_k - q_{k'}). \end{aligned} \quad (2.6)$$

MM used action-angle variables for the electronic dofs because they were implementing the model within the (very crude) “quasiclassical” procedure, whereby the initial conditions (at $t=0$) for the action variables were $n_i(0)=1$ for the initial electronic state i , $n_k(0)=0$ for all other states $k \neq i$, and with all angle variables chosen to be $2\pi * \text{random number}$. The final values of the action variables resulting from com-

putting classical trajectories (in the full nuclear+electronic set of variables) with these initial conditions and this Hamiltonian were then histogrammed in the typical quasiclassical procedure.

Even though MM specified initial conditions in terms of action-angle variables as noted above, they typically transformed to Cartesian electronic variables to carry out the calculations (because they are simpler and better behaved numerically). Defining the electronic oscillator coordinates and momenta in the usual way,

$$\begin{aligned}x_k &= \sqrt{2n_k + 1} \cos(q_k), \\ p_k &= -\sqrt{2n_k + 1} \sin(q_k),\end{aligned}\quad (2.7)$$

the Hamiltonian of Eq. (2.6) becomes

$$\begin{aligned}H(\mathbf{P}, \mathbf{R}, \mathbf{p}, \mathbf{x}) &= \frac{\mathbf{P}^2}{2\mu} + \sum_{k=1}^N V_{kk}(\mathbf{R}) \frac{1}{2}(p_k^2 + x_k^2 - 1) \\ &+ \sum_{k < k'=1}^N V_{kk'}(\mathbf{R})(p_k p_{k'} + x_k x_{k'}),\end{aligned}\quad (2.8)$$

and this is precisely the Hamiltonian that ST (Ref. 7) obtained by a different, more rigorous procedure. Furthermore, the derivation by ST makes it clear that this *model* is actually an exact *representation* of the vibronic system so that if the Hamiltonian of Eq. (2.8) was taken to be a Hamiltonian *operator* in the usual way, then exact vibronic dynamics would be obtained from the resulting Schrödinger equation. The only approximation is therefore the SC-IVR approximation itself, which is summarized in the next section.

An interesting observation from this classical vibronic Hamiltonian, Eq. (2.8), concerns the force that the nuclei experience along a classical trajectory. The Newtonian version of the classical equations of motion gives

$$\begin{aligned}\mu \ddot{\mathbf{R}}(t) &= - \sum_{k=1}^N \frac{1}{2}(p_k^2 + x_k^2 - 1) \frac{\partial V_{kk}(\mathbf{R})}{\partial \mathbf{R}} \\ &- \sum_{k < k'=1}^N (p_k p_{k'} + x_k x_{k'}) \frac{\partial V_{kk'}(\mathbf{R})}{\partial \mathbf{R}}\end{aligned}\quad (2.9)$$

or if this is expressed in terms of the original electronic amplitudes c_k it reads

$$\mu \ddot{\mathbf{R}}(t) = - \sum_{k, k'=1}^N c_k^* \frac{\partial V_{kk'}(\mathbf{R})}{\partial \mathbf{R}} c_{k'},\quad (2.10)$$

which is recognized to be the Ehrenfest force. The traditional Ehrenfest model would choose initial conditions for the amplitudes as $c_i(0)=1$ for the initial state i and $c_k(0)=0$ for all other states much like the quasiclassical model originally used by MM. For the SC-IVR described in the next section, however, the initial conditions for the electronic degrees of freedom are specified by the initial electronic-oscillator wave function in coordinate space x_k . Therefore, for initial electronic state i , the initial oscillator for that mode has one quantum of excitation, and all the other modes $k \neq i$ have zero quanta of excitation (corresponding to the ground state).

The initial electronic-oscillator wave function for the i th electronic state is thus

$$\Phi_i(x_1 \cdots x_N) = \phi_1(x_i) \prod_{k=1, k \neq i}^N \phi_0(x_k) = \frac{\sqrt{(2)^N}}{\pi^{N/4}} x_i e^{-(1/2)x_i^2},\quad (2.11)$$

Finally, we note that the classical vibronic Hamiltonian in Eq. (2.8) is that for the *diabatic* electronic representation, and there is an analogous one for the *adiabatic* representation. In terms of Cartesian coordinates and momentum of the electronic oscillators [as in Eq. (2.8)], it is

$$H(\mathbf{P}, \mathbf{R}, \mathbf{p}, \mathbf{x}) = \sum_{k=1}^N \frac{1}{2}(p_k^2 + x_k^2 - 1) E_k(\mathbf{R}) + \frac{|\mathbf{P} + \Delta \mathbf{P}|^2}{2\mu},\quad (2.12)$$

where $E_k(\mathbf{R})$ are the usual adiabatic or Born-Oppenheimer potential energy surfaces, and $\Delta \mathbf{P}$ is given by

$$\Delta \mathbf{P} = \sum_{k < k'=1}^N \hbar \left\langle \psi_k \left| \frac{\partial \psi_{k'}}{\partial \mathbf{R}} \right. \right\rangle (x_k p_{k'} - x_{k'} p_k),\quad (2.13)$$

where the electronic matrix elements in Eq. (2.13) are the usual nonadiabatic derivative coupling.

III. SEMICLASSICAL INITIAL VALUE REPRESENTATION

The SC-IVR approach⁵ has been reviewed a number of times, so we only summarize here what is necessary for the applications described in Sec. IV. Thus, the coherent state IVR of Herman-Kluk for the time evolution operator is given as an integral over the phase space of initial conditions of classical trajectories,

$$\begin{aligned}e^{-i\hat{H}t/\hbar} &= \frac{1}{(2\pi\hbar)^F} \int d\mathbf{p}_0 \int d\mathbf{q}_0 C_t(p_0, q_0) e^{(i\hbar)S_t} |\mathbf{p}_t, \mathbf{q}_t\rangle \\ &\times \langle \mathbf{p}_0, \mathbf{q}_0 |,\end{aligned}\quad (3.1)$$

where $|\mathbf{p}, \mathbf{q}\rangle$ are coherent states, whose wave function is

$$\langle \mathbf{q}' | \mathbf{p}, \mathbf{q} \rangle = \left(\frac{\gamma}{\pi} \right)^{F/4} e^{[-(\gamma/2)(\mathbf{q}' - \mathbf{q})^2 + (i\hbar)\mathbf{p} \cdot (\mathbf{q}' - \mathbf{q})]},\quad (3.2)$$

and $(\mathbf{p}_t, \mathbf{q}_t)$ are the coordinates and momenta at time t that evolve along the classical trajectory from initial conditions $(\mathbf{p}_0, \mathbf{q}_0)$. $S_t(\mathbf{p}_0, \mathbf{q}_0)$ is the action for this trajectory, and $C_t(\mathbf{p}_0, \mathbf{q}_0)$ the Herman-Kluk prefactor that involves the various monodromy matrix elements,

$$C_t(\mathbf{p}_0, \mathbf{q}_0) = \left| \frac{1}{2} \left(\mathbf{M}_{qq} + \mathbf{M}_{pp} + \frac{\hbar\gamma}{i} \mathbf{M}_{qp} + \frac{i}{\hbar\gamma} \mathbf{M}_{pq} \right) \right|^{1/2},\quad (3.3)$$

where

$$\mathbf{M}_{qq} = \frac{\partial \mathbf{q}_t}{\partial \mathbf{q}_0}, \quad \mathbf{M}_{pp} = \frac{\partial \mathbf{p}_t}{\partial \mathbf{p}_0}, \quad (3.4)$$

$$\mathbf{M}_{qp} = \frac{\partial \mathbf{q}_t}{\partial \mathbf{p}_0}, \quad \mathbf{M}_{pq} = \frac{\partial \mathbf{p}_t}{\partial \mathbf{q}_0}.$$

In the limit that the coherent state parameter $\gamma \rightarrow \infty$, the coherent states become proportional to Dirac position eigenstates, and Eq. (3.1) becomes the original ‘‘Van Vleck’’ IVR,

$$e^{-i\hat{H}t/\hbar} = \frac{1}{(2\pi i\hbar)^{F/2}} \int d\mathbf{p}_0 \int d\mathbf{q}_0 |\mathbf{M}_{qp}|^{1/2} e^{(i/\hbar)S_t} |\mathbf{q}_t\rangle \langle \mathbf{q}_0|. \quad (3.5)$$

For most applications to large molecular systems and for the applications in Sec. IV, one is interested in using the SC-IVR to calculate time correlation functions of the form

$$C_{AB}(t) = \text{tr}[\hat{A} e^{i\hat{H}t} \hat{B} e^{-i\hat{H}t}]. \quad (3.6)$$

Direct use of Eq. (3.1) or (3.5) would thus lead to a *double* phase space average on initial conditions, so various approximations to this have been developed which are easier to implement and thus more applicable to large molecular systems. We consider three such approaches in this paper, summarized here in terms of increasing accuracy.

A. The linearized SC-IVR approximation

If one uses the coordinate space IVR, Eq. (3.5), for the two propagators in the correlation function, Eq. (3.6), and then approximates the integrand by expanding all quantities to first order in the difference of two sets of initial conditions, then the classical Wigner model⁹ is obtained,

$$C_{AB}(t) = (2\pi\hbar)^{-F} \int d\mathbf{p}_0 \int d\mathbf{q}_0 A_w(\mathbf{p}_0, \mathbf{q}_0) B_w(\mathbf{p}_t, \mathbf{q}_t), \quad (3.7)$$

where A_w and B_w are the Wigner functions corresponding to operators \hat{A} and \hat{B} , respectively, e.g.,

$$A_w(\mathbf{p}, \mathbf{q}) = \int d\Delta \mathbf{q} e^{-i\mathbf{p}^T \cdot \Delta \mathbf{q} / \hbar} \left\langle \mathbf{q} + \frac{\Delta \mathbf{q}}{2} \middle| \hat{A} \middle| \mathbf{q} - \frac{\Delta \mathbf{q}}{2} \right\rangle. \quad (3.8)$$

This LSC-IVR/classical Wigner model is an old idea and has been around for a long time; the interest here is seeing that it is contained within the SC-IVR, being a (rather crude) approximation to it (and there are even other, more recent derivations of the Wigner model from other starting points).^{10,11} One sees that it has precisely the form of the classical time correlation function, only with the classical functions corresponding to operators \hat{A} and \hat{B} replaced by their Wigner functions.

B. The forward-backward IVR

Though the LSC-IVR/classical Wigner model is able to describe some of the quantum aspects of the dynamics, it cannot describe true quantum coherence features (as will be illustrated in Sec. IV). The simplest IVR approach known at present which can do so is the FB-IVR, as described by

Miller.¹² To illustrate it we state the result for the case that operator \hat{B} in Eq. (3.6) involves only the momentum operator(s) in the following manner

$$\hat{B} = e^{i\Phi(\hat{\mathbf{p}})}. \quad (3.9)$$

The FB-IVR then gives the correlation function as a *single* phase space average over initial conditions,

$$C_{AB}(t) = (2\pi\hbar)^{-F} \int d\mathbf{p}_0 \int d\mathbf{q}_0 C_0(\mathbf{p}_0, \mathbf{q}_0) \times e^{iS_0(\mathbf{p}_0, \mathbf{q}_0)/\hbar} \langle \mathbf{p}_0, \mathbf{q}_0 | \hat{A} | \mathbf{p}'_0, \mathbf{q}'_0 \rangle. \quad (3.10)$$

The forward-backward trajectory begins at $t=0$ with initial conditions $(\mathbf{p}_0, \mathbf{q}_0)$, evolves to time t , at which point it undergoes a jump in position (with no change in the momentum \mathbf{p}_t),

$$\mathbf{q}_t \rightarrow \mathbf{q}_t - \frac{\partial \Phi(\mathbf{p}_t)}{\partial \mathbf{p}_t}, \quad (3.11)$$

and then evolves backward in time to $t=0$; $(\mathbf{p}'_0, \mathbf{q}'_0)$ is the final phase point reached. The net FB action $S_0(\mathbf{p}_0, \mathbf{q}_0)$ in Eq. (3.10) is

$$S_0(\mathbf{p}_0, \mathbf{q}_0) = \int_0^t dt' [\mathbf{p} \cdot \dot{\mathbf{q}} - H(\mathbf{p}, \mathbf{q})] + \Delta S + \int_t^0 dt' [\mathbf{p} \cdot \dot{\mathbf{q}} - H(\mathbf{p}, \mathbf{q})], \quad (3.12)$$

where

$$\Delta S = -\mathbf{p}_t \cdot \frac{\partial \Phi(\mathbf{p}_t)}{\partial \mathbf{p}_t} + \Phi(\mathbf{p}_t). \quad (3.13)$$

We note here that if $\Phi(\hat{\mathbf{p}})$ is a linear function, then ΔS is zero. The prefactor takes the same form as before in Eq. (3.3).

The FB-IVR comes from making a stationary phase approximation at time t , is an important result that reduces the double phase space average over initial conditions to a single such average, and is thus very much the same level of complexity as the LSC-IVR described above (although over the more complicated FB trajectory). A number of applications have shown that the FB-IVR can indeed describe true quantum coherence effects.¹³

C. An exact FB-IVR

It has been shown by one of us how an ‘‘exact’’ FB-type IVR [Ref. 5(c)] can be constructed, exact in the sense that it involves no approximation other than the basic IVR expression for the propagator itself, e.g., Eq. (3.1) or (3.5). Here we show how this works for the special case that operator \hat{B} is a function only of the momentum operator(s), $\hat{B} = B(\hat{\mathbf{p}})$, as will be the case for the applications in Sec. IV. For this purpose we use the generalized HK-IVR given by Kay,¹⁴ where the coherent state parameter gamma is allowed to be different for time 0 and time t . Equations (3.1)–(3.3) thus give the two time evolution operators as

$$e^{-i\hat{H}t/\hbar} = (2\pi\hbar)^{-F} \int d\mathbf{q}_0 \int d\mathbf{p}_0 C_t(\mathbf{q}_0, \mathbf{p}_0; \gamma_o, \gamma_t) e^{(i/\hbar)S_t(\mathbf{q}_0, \mathbf{p}_0)} \times |\mathbf{p}_t, \mathbf{q}_t; \gamma_t\rangle \langle \mathbf{p}_o, \mathbf{q}_o; \gamma_o|, \quad (3.14)$$

$$e^{i\hat{H}t/\hbar} = (2\pi\hbar)^{-F} \int d\mathbf{q}'_t \int d\mathbf{p}'_t C_{-t}(\mathbf{q}'_t, \mathbf{p}'_t; \gamma'_o, \gamma'_t) \times e^{(i/\hbar)S_{-t}(\mathbf{q}'_t, \mathbf{p}'_t)} |\mathbf{p}'_o, \mathbf{q}'_o; \gamma'_o\rangle \langle \mathbf{p}'_t, \mathbf{q}'_t; \gamma'_t|. \quad (3.15)$$

The expression for the time correlation function thus becomes

$$C_{AB}(t) = (2\pi\hbar)^{-2F} \int d\mathbf{q}_0 \int d\mathbf{p}_0 \int d\mathbf{q}'_t \int d\mathbf{p}'_t \times C_{-t}(\mathbf{q}'_t, \mathbf{p}'_t; \gamma'_o, \gamma'_t) C_t(\mathbf{q}_0, \mathbf{p}_0; \gamma_o, \gamma_t) \times \langle \mathbf{p}'_t, \mathbf{q}'_t; \gamma'_t | \hat{B} | \mathbf{p}_t, \mathbf{q}_t; \gamma_t \rangle e^{(i/\hbar)S_t(\mathbf{q}_0, \mathbf{p}_0)} e^{(i/\hbar)S_{-t}(\mathbf{q}'_t, \mathbf{p}'_t)} \times \langle \mathbf{p}_o, \mathbf{q}_o; \gamma_o | \hat{A} | \mathbf{p}'_o, \mathbf{q}'_o; \gamma'_o \rangle. \quad (3.16)$$

To take advantage of the fact that operator $\hat{B}=B(\hat{\mathbf{p}})$ and its momentum space matrix thus diagonal, one then takes the momentum space limit for the coherent state parameters γ_t and γ'_t , whereby Eq. (3.16) becomes

$$C_{AB}(t) = (2\pi\hbar)^{-F} \int d\mathbf{q}_0 \int d\mathbf{p}_0 \int d\mathbf{q}'_t \times \mathcal{D}_t^f(\mathbf{q}_0, \mathbf{p}_0; \gamma_o) \mathcal{D}_{-t}^b(\mathbf{q}'_t, \mathbf{p}_t; \gamma'_o) B(\mathbf{p}_t) \times e^{(i/\hbar)S_t(\mathbf{q}_0, \mathbf{p}_0)} e^{(i/\hbar)S_{-t}(\mathbf{q}'_t, \mathbf{p}_t)} e^{(i/\hbar)\mathbf{p}_t \cdot (\mathbf{q}'_t - \mathbf{q}_t)} \times \langle \mathbf{p}_o, \mathbf{q}_o; \gamma_o | \hat{A} | \mathbf{p}'_o, \mathbf{q}'_o; \gamma'_o \rangle, \quad (3.17)$$

where the two prefactor matrix elements are

$$\mathcal{D}_t^f(\mathbf{q}_0, \mathbf{p}_0; \gamma_o) = \left| \frac{1}{2\sqrt{\pi}} \left(\mathbf{M}_{pp} \gamma_o^{1/2} + \frac{i}{\hbar} \mathbf{M}_{pq} \gamma_o^{-1/2} \right) \right|^{1/2}, \quad (3.18)$$

$$\mathcal{D}_{-t}^b(\mathbf{q}'_t, \mathbf{p}_t; \gamma'_o) = \left| \frac{1}{2\sqrt{\pi}} \left(\gamma_o'^{1/2} \mathbf{M}'_{qq} + \frac{i}{\hbar} \gamma_o'^{-1/2} \mathbf{M}'_{pq} \right) \right|^{1/2}.$$

IV. APPLICATIONS

Calculations have been carried out for model systems consisting of two electronic states and one nuclear degree of freedom (translation), the same kind of models Tully used earlier for testing various surface-hopping approaches. A diabatic electron matrix $V_{nn'}(R), n, n'=1, 2$, characterizes the two electronic states. The overall system thus consists of three degrees of freedom, for which the classical vibronic Hamiltonian of Eq. (2.8) is

$$H(P, R, p_1, x_1, p_2, x_2) = \frac{P^2}{2\mu} + V_{11}(R) \frac{1}{2}(p_1^2 + x_1^2 - 1) + V_{22}(R) \frac{1}{2}(p_2^2 + x_2^2 - 1) + V_{12}(R)(p_1 p_2 + x_1 x_2). \quad (4.1)$$

Figures 1 and 2 show the diabatic (and also the adiabatic) potential functions for the two specific models that are

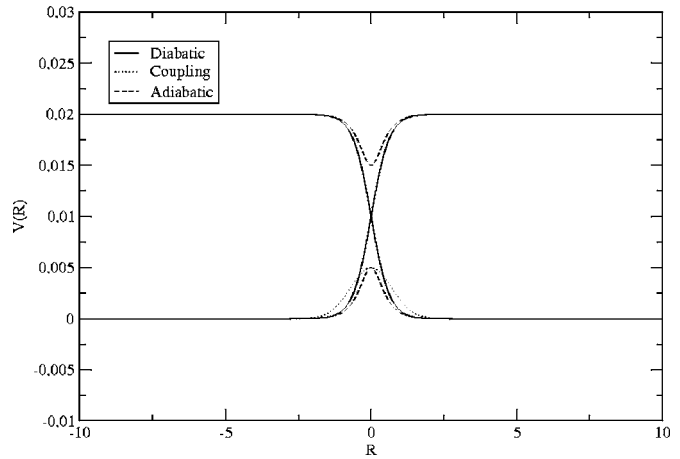


FIG. 1. The potential curves in both diabatic and adiabatic representations for model 1.

treated; the specific forms of the diabatic electronic matrix for model 1 are

$$V_{11}(R) = V_0 \tanh(aR), \quad V_{22}(R) = -V_0 \tanh(aR), \quad (4.2)$$

$$V_{12}(R) = C e^{-DR^2},$$

and for model 2 are

$$V_{11}(R) = V_1 \tanh(aR), \quad V_{22}(R) = -V_2 \tanh(aR), \quad V_1 \gg V_2, \quad (4.3)$$

$$V_{12}(R) = C e^{-D(R+f)^2}.$$

Model 1 is identical to one of the examples Tully used, and the parameters used here are $V_0=0.01$, $a=1.6$, $C=0.005$, and $D=1$. Model 2 is an asymmetric system where one channel has a very high energetic threshold and the parameters used in this case are $V_1=0.04$, $V_2=0.01$, $C=0.005$, $D=1$, and $f=0.7$.

The quantity calculated in all cases is the *probability distribution of final nuclear translational momentum*, which

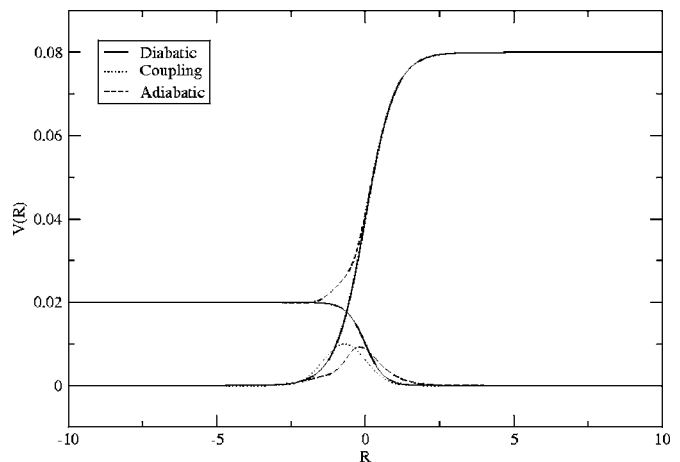


FIG. 2. The potential curves in both diabatic and adiabatic representations for model 2.

can be expressed as the long time limit of the A - B correlation function of Eq. (3.6), where operator \hat{A} is the projection operator for the initial state,

$$|\Psi_i\rangle\langle\Psi_i|, \quad (4.4)$$

and operator \hat{B} is

$$\delta(P_f - \hat{P}). \quad (4.5)$$

The correlation function is, therefore,

$$\begin{aligned} C(P_f; t) &= \lim_{t \rightarrow \infty} \text{tr} [|\Psi_i\rangle\langle\Psi_i| e^{i\hat{H}t} \delta(P_f - \hat{P}) e^{-i\hat{H}t}] \\ &= \lim_{t \rightarrow \infty} \langle\Psi_i| e^{i\hat{H}t} \delta(P_f - \hat{P}) e^{-i\hat{H}t} |\Psi_i\rangle. \end{aligned} \quad (4.6)$$

The initial state is chosen to be a translational coherent state (with a relatively well-defined value of the initial translational momentum) in electronic state 1,

$$\begin{aligned} \Psi_i(x_1, x_2, P, R) &= \left(\frac{\gamma}{\pi}\right)^{1/4} e^{-(\gamma/2)(R - R_i)^2} e^{iP_i(R - R_i)} \\ &\quad \times \left(\frac{2}{\pi}\right)^{1/2} x_1 e^{-(1/2)(x_1^2 + x_2^2)}. \end{aligned} \quad (4.7)$$

The initial position R_i is chosen well to the left of the curve-crossing region ($R_i = -5$), and the initial momentum is positive, with trajectories headed toward the crossing region.

For the LSC-IVR/classical Wigner approximation of Sec. III A, it is necessary to calculate the Wigner function for operator \hat{A} ; this can be done analytically in this case, giving

$$\begin{aligned} A_w &= (|\Psi_i\rangle\langle\Psi_i|)_w \\ &= (2)^3 e^{-\gamma(R - R_i)^2} e^{-(1/\gamma)(P - P_i)^2} e^{-(x_1^2 + p_1^2 + x_2^2 + p_2^2)} \\ &\quad \times (2x_1^2 + 2p_1^2 - 1). \end{aligned} \quad (4.8)$$

Operator \hat{B} remains unchanged under the Wigner transformation.

For the FB-IVR of Sec. III B, one Fourier expands the delta function of operator \hat{B} , so that Eq. (4.6) becomes

$$C(P_f; t) = (2\pi\hbar)^{-1} \int_{-\infty}^{\infty} d\bar{R} e^{i\bar{R}P_f/\hbar} \langle\Psi_i| e^{i\hat{H}t} e^{-i\hat{P}\bar{R}/\hbar} e^{-i\hat{H}t} |\Psi_i\rangle, \quad (4.9)$$

and the FB-IVR is used to evaluate $\tilde{P}(\bar{R})$,

$$\begin{aligned} \tilde{P}(\bar{R}) &\equiv \langle\Psi_i| e^{i\hat{H}t} e^{-i\hat{P}\bar{R}/\hbar} e^{-i\hat{H}t} |\Psi_i\rangle \\ &= (2\pi\hbar)^{-F} \int d\mathbf{p}_0 \int d\mathbf{q}_0 \langle\Psi_i| \mathbf{p}'_0, \mathbf{q}'_0 \rangle \\ &\quad \times \langle\mathbf{p}_0, \mathbf{q}_0 | \Psi_i \rangle C_0(\mathbf{q}_0, \mathbf{p}_0) e^{iS_0(\mathbf{q}_0, \mathbf{p}_0)/\hbar}. \end{aligned} \quad (4.10)$$

The FB trajectory for Eq. (4.10) begins with initial conditions $(\mathbf{p}_0, \mathbf{q}_0)$, evolves to time t at which the translational coordinate undergoes a jump in the nuclear coordinate $R_t \rightarrow R_t + \bar{R}$, and then propagates back to time 0, $(\mathbf{p}'_0, \mathbf{q}'_0)$ being the final values. Once $\tilde{P}(\bar{R})$ is thus calculated by this FB-IVR procedure, its Fourier transform gives $C(P_f; t)$ by Eq. (4.9).

The exact FB-IVR expression in this case is

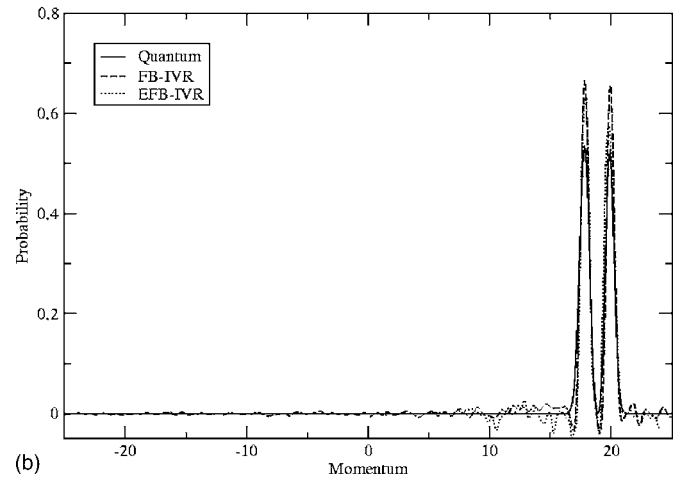
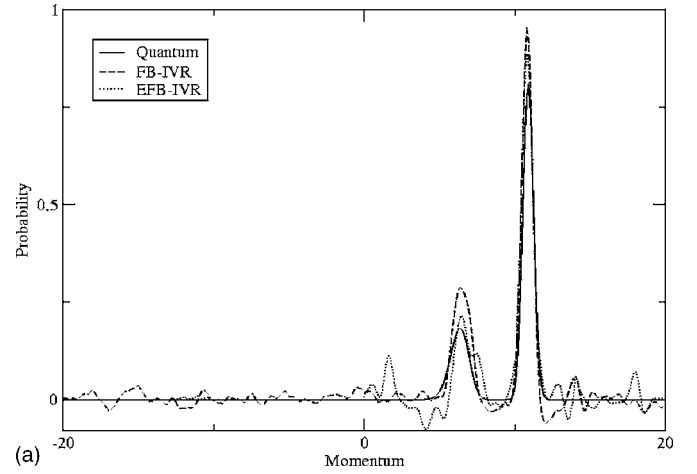


FIG. 3. (a) Comparison of results of FB-IVR, exact FB-IVR, and exact quantum calculations for model 1 with an initial energy of 0.03 hartree. (b) Comparison of results of FB-IVR, exact FB-IVR, and exact quantum calculations for model 1 with an initial energy of 0.1 hartree.

$$\begin{aligned} C(P_f; t) &= (2\pi\hbar)^{-F} \int d\mathbf{q}_0 \int d\mathbf{p}_0 \int d\mathbf{q}'_t \mathcal{D}_t^f(\mathbf{q}_0, \mathbf{p}_0; \gamma_o) \\ &\quad \times \mathcal{D}_t^b(\mathbf{q}'_t, \mathbf{p}_t, \gamma'_o) \delta(p'_t - P_f) \\ &\quad \times e^{(i\hbar)S_t(\mathbf{q}_0, \mathbf{p}_0)} e^{(i\hbar)S_t(\mathbf{q}'_t, \mathbf{p}_t)} e^{(i\hbar)\mathbf{p}_t \cdot (\mathbf{q}'_t - \mathbf{q}_t)} \\ &\quad \times \langle\Psi_i| \mathbf{p}'_o, \mathbf{q}'_o; \gamma'_o \rangle \langle\mathbf{p}_o, \mathbf{q}_o; \gamma_o | \Psi_i\rangle. \end{aligned} \quad (4.11)$$

The trajectory has the same forward-backward structure as in the FB-IVR case. However, the position jump at time t is over both the nuclear and the electronic coordinates.

V. RESULTS AND DISCUSSION

First, Figs. 3(a) and 3(b) show the results of the FB-IVR and the EFB-IVR compared with exact quantum results for model 1, at two incident translational energies, 0.03 and 0.1 hartree, respectively. These distributions show two peaks at positive momentum, corresponding to the two electronic states in which the system may emerge. The peaks have finite width because the initial translational wave function has a (small) spread in translational energy. The area under the peaks gives the transition probabilities from the initial elec-

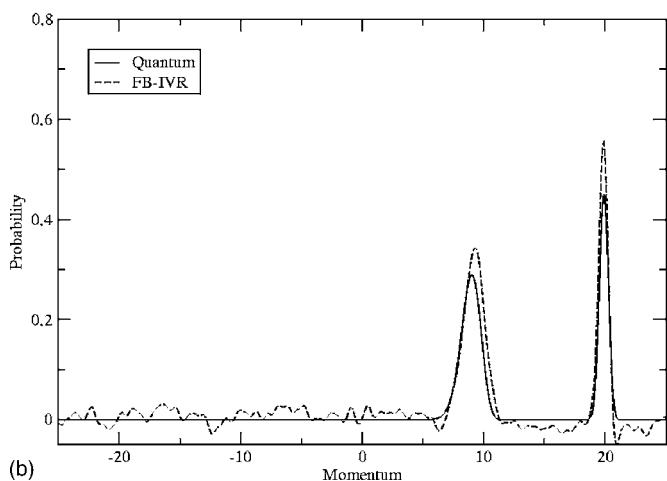
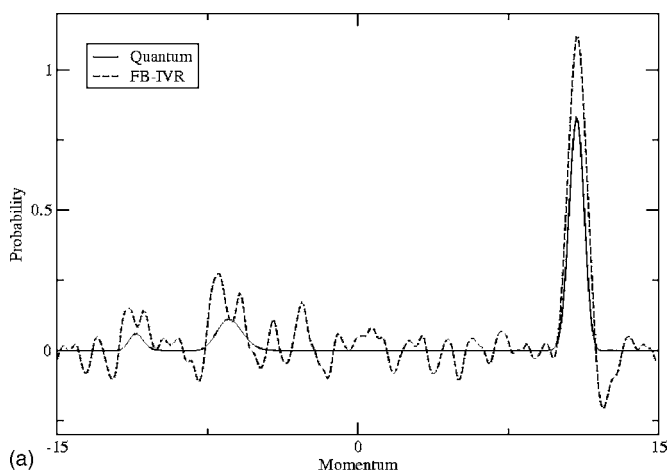


FIG. 4. (a) Comparison of results of FB-IVR and exact quantum calculations for model 2 with an initial energy of 0.03 hartree. (b) Comparison of results of FB-IVR and exact quantum calculations for model 2 with an initial energy of 0.1 hartree.

tronic state to the two possible final states, either for transmission ($P_f > 0$) or reflection ($P_f < 0$). The basic conclusion from Figs. 3(a) and 3(b) is that the FB-IVR and EFB-IVR both describe the process semiquantitatively, with the FB-IVR showing less numerical noise than the EFB-IVR (at least with our present calculations).

Figures 4(a) and 4(b) show the results of the FB-IVR calculations, compared to the exact quantum results, for model 2 at the same two translational energies. At the lower energy [Fig. 4(a)], the excited electronic state is energetically forbidden (i.e., it is a closed channel) in transmission ($P_f > 0$), but both states are open for reflection ($P_f < 0$); the FB-IVR (and quantum result) correctly shows one peak for positive momentum and two peaks for negative momentum. And again, the FB-IVR agrees well with the correct quantum result. At the higher energy [Fig. 4(b)], both electronic states are open in transmission, and one sees two peaks for positive momentum and essentially no peaks corresponding to reflected transitions.

Figures 5(a), 5(b), 6(a), and 6(b) show the results of the classical Wigner/LSC-IVR model and also the standard Ehrenfest model, for models 1 and 2, for two initial nuclear translational energies, 0.03 and 0.1 hartree. One sees in Figs.

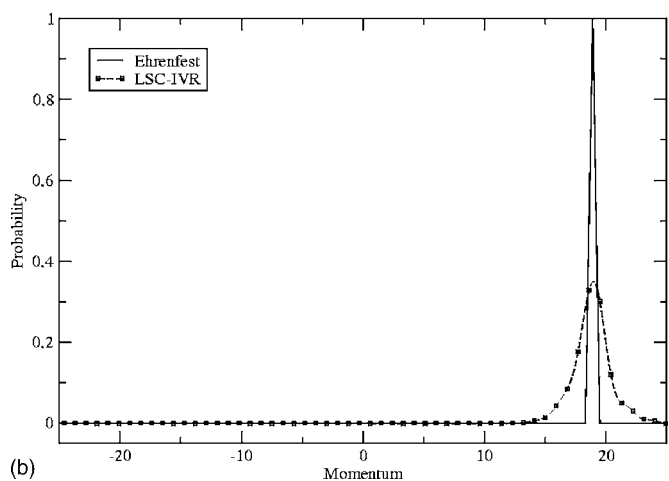
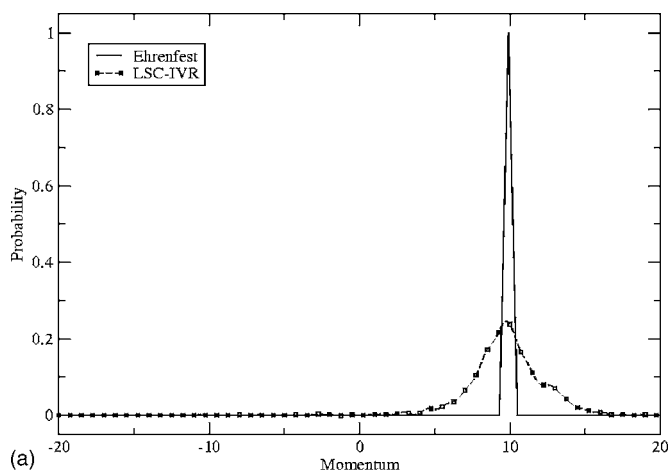
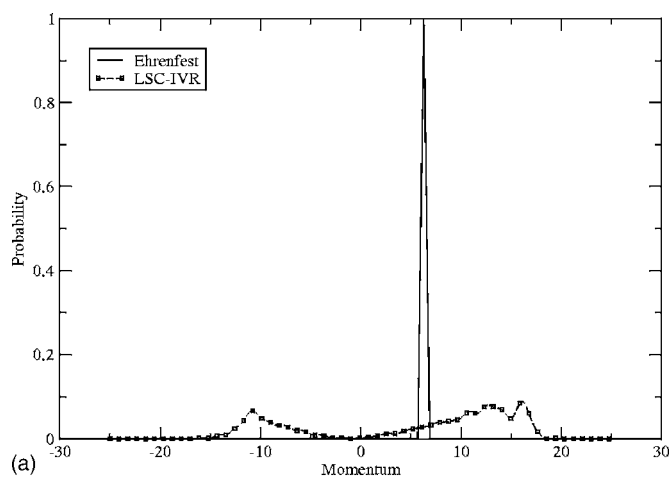
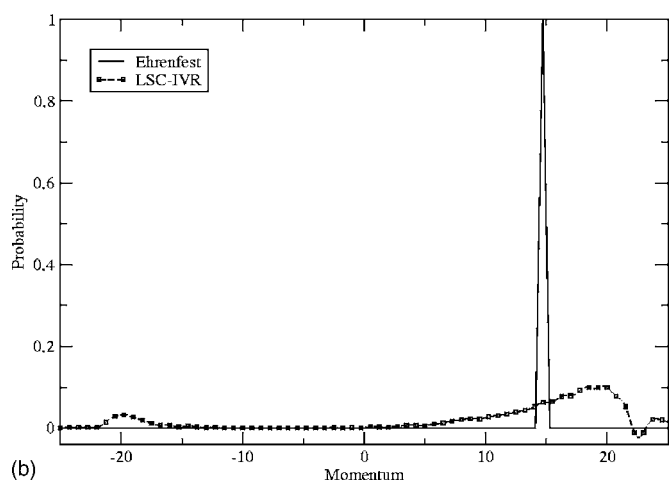


FIG. 5. (a) Linearized IVR and Ehrenfest results for model 1. Initial energy=0.03 hartree. (b) Linearized IVR and Ehrenfest results for model 1. Initial energy=0.1 hartree.

5(a) and 5(b) (model 1) that for each energy there is only a single peak in the translational energy distribution, clearly demonstrating that the translational motion has emerged on an average electronic potential curve, not one curve or the other. One also sees that the classical Wigner/LSC-IVR model is essentially the same as the standard Ehrenfest model, the primary difference being that since the initial conditions for the electronic variables have a distribution (the Wigner distribution) in values—while there is no distribution in the initial electronic variables in the standard Ehrenfest model—there is a broadening in the very sharp peak given by the Ehrenfest model. (The Ehrenfest peak is, in fact, a delta function, so its width in Figs. 5 and 6 is for visual purposes only.) Figures 6(a) and 6(b) show similar behavior for model 2; here the distribution given by the classical Wigner model is *extremely* broad for the lower energy case because here there is a significant probability of reflection ($P_f < 0$) as well as transmission. The results in both Figs. 5(a), 5(b), 6(a), and 6(b) verify the unphysical behavior of the Ehrenfest model and that the LSC-IVR/classical Wigner model is essentially equivalent to it. These shortcomings are due to the fact that these models cannot describe quantum



(a)



(b)

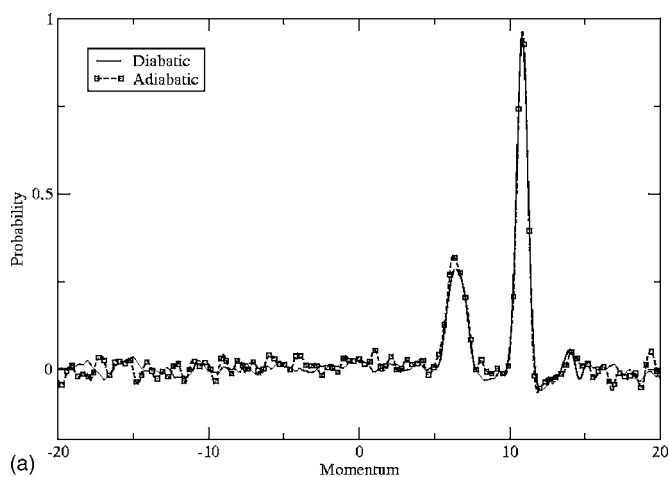
FIG. 6. (a) Linearized IVR and Ehrenfest results for model 2. Initial energy=0.03 hartree. (b) Linearized IVR and Ehrenfest results for model 2. Initial energy=0.1 hartree.

coherence/interference effects, which are necessary to properly quantize the electronic degrees of freedom.

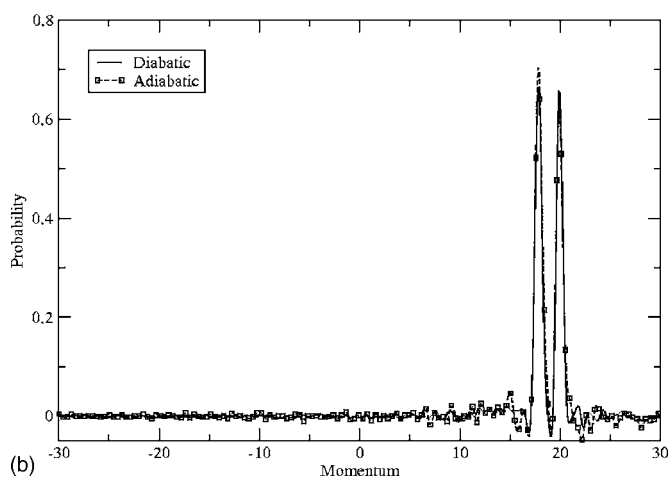
Finally, Figs. 7(a) and 7(b) show FB-IVR calculations for model 1 at the two energies, comparing the results given by using the diabatic electronic representation (as did all calculations above) and the adiabatic electronic representation [with Hamiltonian given by Eq. (2.12)]. The results should, of course, be the same, and within an extremely small numerical error, they are.

VI. CONCLUDING REMARKS

The SC-IVR and LSC-IVR along with the MM-ST Hamiltonian have already been shown to be useful in the study of nonadiabatic dynamics. In this paper, we further show the effectiveness of the FB-IVR, which allows us to better evaluate quantities that involve double phase space integrals. We further discuss the application of the LSC-IVR and compare it favorably to the Ehrenfest model. We also demonstrate the representation independent nature of our methods. It is important to note that both the FB-IVR and LSC-IVR are more feasible for extension to multidimensional systems and, in particular, the ability of FB-IVR to



(a)



(b)

FIG. 7. (a) Comparison of the adiabatic and diabatic results for model 1, with an initial energy of 0.03 hartree. (b) Comparison of the adiabatic and diabatic results for model 1, with an initial energy of 0.1 hartree.

model nonadiabatic dynamics almost exactly shows that there need be no compromise on the incorporation of quantum effects in order to do so.

ACKNOWLEDGMENTS

This work was supported by the Office of Naval Research Grant No. N00014-07-1-0586 and by the Director, Office of Science, Office of Basic Energy Sciences, Chemical Sciences, Geosciences, and Biosciences Division, U.S. Department of Energy under Contract No. DE-AC02-05CH11231.

- ¹J. C. Tully, *J. Chem. Phys.* **93**, 1061 (1990); X. Li, J. C. Tully, H. B. Schlegel, and M. J. Frisch, *ibid.* **123**, 084106 (2005); P. V. Parandekar and J. C. Tully, *J. Chem. Theory Comput.* **2**, 229 (2006).
- ²E. Neria and A. Nitzan, *J. Chem. Phys.* **99**, 1109 (1993).
- ³O. V. Prezhdo and P. J. Rossky, *J. Chem. Phys.* **107**, 825 (1997).
- ⁴M. D. Hack and D. G. Truhlar, *J. Chem. Phys.* **114**, 2894 (2001).
- ⁵(a) W. H. Miller, *J. Phys. Chem. A* **105**, 2942 (2001); (b) W. H. Miller, *Proc. Natl. Acad. Sci. U.S.A.* **102**, 6660 (2005); (c) W. H. Miller, *J. Chem. Phys.* **125**, 132305 (2006).
- ⁶H.-D. Meyer and W. H. Miller, *J. Chem. Phys.* **70**, 3214 (1979).
- ⁷G. Stock and M. Thoss, *Phys. Rev. Lett.* **78**, 578 (1997).
- ⁸X. Sun and W. H. Miller, *J. Chem. Phys.* **106**, 6346 (1997).
- ⁹X. Sun, H. B. Wang, and W. H. Miller, *J. Chem. Phys.* **109**, 4190 (1998); **109**, 7064 (1998); W. H. Miller, *J. Phys. Chem. A* **103**, 9384 (1999).
- ¹⁰J. L. Liao and E. Pollak, *J. Chem. Phys.* **108**, 2733 (1998).

- ¹¹J. A. Poulsen, G. Nyman, and P. J. Rossky, *J. Chem. Phys.* **119**, 12179 (2003).
- ¹²W. H. Miller, *Faraday Discuss. Chem. Soc.* **110**, 1 (1998); X. Sun and W. H. Miller, *J. Chem. Phys.* **110**, 6635 (1999).
- ¹³H. Wang, M. Thoss, K. Sogge, R. Gelabert, X. Gimenez, and W. H. Miller, *J. Chem. Phys.* **114**, 2562 (2001); R. Gelabert, X. Gimenez, M. Thoss, H. Wang, and W. H. Miller, *ibid.* **114**, 2572 (2001).
- ¹⁴K. G. Kay, *J. Chem. Phys.* **100**, 4377 (1994); **100**, 4432 (1994).